J Therm Anal Calorim (2012) 108:1213–1222
DOI 10.1007/s10973-011-1826-9

Thermal and kinetic analysis of uranium salts

Part 1. Uranium (VI) oxalate hydrates

Halil Cetişli · Gülbanu Koyundereli Çılgı · Ramazan Donat

Received: 13 April 2011 / Accepted: 27 July 2011 / Published online: 13 August 2011

Abstract The thermal decomposition kinetics of $UO_2C_2O_4{\cdot}3H_2O$ were studied by TG method in a flowing nitrogen, air, and oxygen atmospheres. It is found that $UO_2C_2O_4{\cdot}3H_2O$ decomposes to uranium oxides in four stages in all atmosphere. The first two stages are the same in the whole atmosphere that correspond to dehydration reactions. The last two stages correspond to decomposition reactions. Final decomposition products are determined with X-Ray powder diffraction method. Decomposition mechanisms are different in nitrogen atmosphere from air and oxygen atmosphere. The activation energies of all reactions were calculated by model-free (KAS and FWO) methods. For investigation of reaction models, 13 kinetic model equations were tested and correct models, giving the highest linear regression, lowest standard deviation, and agreement of activation energy value to those obtained from KAS and FWO equations were found. The optimized value of activation energy and Arrhenius factor were calculated with the best model equation. Using these values, thermodynamic functions (ΔH^*, ΔS^*, and ΔG^*) were calculated.

Keywords Uranyl oxalate · Thermal decomposition · Kinetic analysis · TG · Kinetic model

Introduction

Complexes of uranyl ion with the simplest organic ligand containing carbonyl group, the oxalate ion, have also attracted a great deal of interest because of their great versatility, the important role of the oxalic acid as precipitating agent in the nuclear fuel technology or waste decontamination purpose or complexing agent to adjust extracting characteristics of actinides and lanthanides or redox behavior of actinides [1].

Aybers synthesized thorium oxalate dihydrate salt and investigated thermal decomposition reactions of this salt using TG–DTA techniques. In this study, decompositions were investigated in five stages. First two stages correspond to dehydration and the other stages correspond to decomposition. The author found that anhydrite thorium oxalate decomposes to ThO_2 by proceeding through the formation of thorium carbonate and thorium oxy-carbonate intermediate products. The kinetic parameters of all reactions were calculated by Coats Redfern method [2].

Different crystal formulas were described such as $UO_2C_2O_4{\cdot}3H_2O$, $[(UO_2)_2C_2O_4(OH)_2{\cdot}(H_2O)_2]H_2O$, and $(UO_2)_2C_2O_4(OH)_2{\cdot}(H_2O)_2$ for uranyl oxalate salts [1]. Dollimore et al. synthesized $UO_2C_2O_4{\cdot}3H_2O$ with three different ways and investigated thermal behavior of this salt. They searched surface area changes due to the isothermal decomposition of this anhydrous salt and found that the surface area increased maximum degree at $\alpha = 0.54$ where α was fractional decomposition. After this result, kinetic studies were limited in the range of $\alpha = 0$–0.5 and the activation energy value were calculated as 240 ± 10 kJ/mol [3].

Tel et al. [4] synthesized uranyl oxalate powders and characterized it by TG/DTG, IR, and X-Ray diffraction methods.

Dahale et al. [5, 6] synthesized lithium uranyl oxalate hydrate, sodium uranyl oxalate hydrate, potassium uranyl oxalate hydrate and was characterized by chemical and thermal analyses as well as X-ray diffraction and infrared

H. Cetişli · G. K. Çılgı (✉) · R. Donat
Department of Chemistry, Faculty of Science and Arts, Pamukkale University, 20070 Denizli, Turkey
e-mail: gkcilgi@gmail.com

spectroscopy. Rodante et al. [7] synthesized $Na_4(UO_2)_2(OH)_4(C_2O_4)_2$ complex salt. They studied thermal decomposition of this salt using Kissinger–Akahira–Sunose (KAS) method.

As noted above, there are a few manuscripts in this field. Also there are disagreements on the decomposition steps of uranyl oxalate, especially about the structure of last oxide products. While Dollimore et al. suggested that U_3O_8 is the final oxide product in air atmosphere, Tel et al. suggested UO_2 as final oxide product under same conditions [3, 4]. Dahale et al. noted that UO_2 and M_2UO_4 have been appeared to be initial and final thermal degradation products of metallic uranyl oxalate salts under argon gas consecutively. When the same experiment has been repeated under air atmosphere due to rapid degradation, they could not observe UO_2 as final product and stated M_2UO_4 as single product [5, 6]. In addition, there is a deficiency in the literature about kinetic analysis of each decomposition stages. This conflict and deficiency have indicated a need for more studies on the thermal decomposition of uranyl oxalate.

In this study, thermal decomposition of $UO_2C_2O_4{\cdot}3H_2O$ compound has been examined in detail from a fresh point of view, and reaction kinetic and thermodynamic parameters were determined. The reaction enthalpy value of dehydration stages were calculated from DSC and DTA peak areas. The activation energy value for each stage are calculated via, KAS, FWO (Flynn–Wall–Ozawa) integral model-free equations. The alterations of activation energies with respect to the decomposition fraction, atmospheric conditions, and the method were investigated. Once the activation energy has been determined, it is possible to find the kinetic model which best describes TG curve of the measurement. Thirteen model equations are used to fit kinetic curves. We used better linear correlation coefficient and agreement of activation energy value to those obtained from model-free equations. The optimized value of activation energy and Arrhenius factor were calculated with the best equation. Using these optimized values, other thermodynamic functions (ΔH^*, ΔS^*, and ΔG^*) were calculated.

Theory

The experimental data for the kinetic analysis of heterogeneous solid–gas reactions can be obtained under different conditions. Here, we analyze the data obtained under non-isothermal conditions, with a linear regime of temperature increase in time ($\beta = dT/dt = \text{const.}$, where β is the heating rate, T is the temperature, and t is the time). Under such conditions, for a heterogeneous solid–gas reaction, which occurs in a single stage, the reaction rate is expressed by the well-known general equation:

$$\frac{\partial \alpha}{\partial T}\beta = Ae^{-E/RT}f(\alpha) \tag{1}$$

where α is the degree of conversion, A is the pre-exponential factor, E is the activation energy, $f(\alpha)$ is the differential conversion function, and R is the gas constant. Equation 1 may also lead to the corresponding equations of the KAS and FWO after integration form [8–12].

KAS equation;

$$\ln\frac{\beta}{T^2} = \left[\ln\frac{AR}{g(\alpha)E}\right] - \frac{E}{R}\frac{1}{T} \tag{2}$$

FWO equation;

$$\ln\beta = \left[\frac{AE}{Rg(\alpha)}\right] - 5.3305 - 1.05178\frac{E}{R}\frac{1}{T} \tag{3}$$

For $\alpha = \text{const.}$, the plot of $\ln\beta/T^2$ versus $1/T$ (for KAS equation), and the plot of $\ln\beta$ versus $1/T$ (for FWO equation), obtained from thermograms, which are recorded at several heating rates, should be a straight line with slope that allows an evaluation of the activation energy.

For determination of reaction kinetic model, we rearranged of KAS and FWO equations as follows which they are known as "Composite Method I" and "Composite Method II" in some literature [13, 14].

Modeling KAS equation (Composite Method I, C.M I);

$$\ln\frac{g(\alpha)}{T^2} = \left[\ln\frac{AR}{\beta E}\right] - \frac{E}{R}\frac{1}{T} \tag{4}$$

Modeling FWO equation (Composite Method II, C.M II);

$$\ln g(\alpha) = \left[\frac{AE}{\beta R}\right] - 5.3305 - 1.05178\frac{E}{R}\frac{1}{T} \tag{5}$$

Hence, the dependence of $\ln[g(\alpha)/T^2]$ (in modeling with KAS method) or $\ln[g(\alpha)]$ (in modeling with FWO method) calculated for different α values at single β value, on $1000/T$ must give rise to a single master straight line for the correct form of $g(\alpha)$. The activation energy and pre-exponential factor value were calculated for each model functions $g(\alpha)$ which are well known in literature [15, 16]. The proper kinetic model function which has highest regression analysis, lowest standard deviation, and the activation energy value shows good agreement to those obtained from model-free KAS and FWO equations was selected.

The entropy of activation, ΔS^*, can be calculated using the equation

$$A = \left(kT_{\text{avg}}/h\right)e^{\Delta S^*/R} \tag{6}$$

where k is the Boltzmann constant, h the Planck's constant, and T_{avg}. is the average reaction temperature.

Since,

$$\Delta H^* = E_a - RT_{avg}. \quad (7)$$

where E_a is the activation energy which is calculated from the slope of Composite methods graphs for proper model. The changes of the enthalpy ΔH^* and Gibbs free energy ΔG^* for the activated complex formation from the reagent can be calculated using the well-known thermodynamic equation:

$$\Delta G^* = \Delta H^* - T_{avg}\Delta S^* \quad (8)$$

Experimental

$UO_2C_2O_4{\cdot}3H_2O$ was synthesized in literature method [5]. All of the thermogravimetry (TG), differential thermogravimetry (DTG), and differential thermal analysis (DTA) curves were obtained simultaneously using a Shimadzu DTG-60H Thermal Analyzer. Differential Scanning Calorimeter (DSC) measurements were performed with Shimadzu DSC-60H device. The measurements were carried out in a flowing nitrogen, oxygen, and air atmosphere and temperature ranged from 25 to 600 °C in an alumina crucible. Highly sintered Al_2O_3 was used as the reference material. The heating rate (β) varied as 6, 4, and 2 °C/min, where the sample mass (w_0) was ranged from 11 to 12 mg. All experiments were performed three times for repeatability, and the results showed good reproducibility with the smaller variations in the kinetic parameters.

The X-Ray powder diffraction patterns were obtained with Rigaku Miniflex X-ray diffractometer, using Cu Kα radiation source.

Results and discussions

Thermal analysis of $UO_2C_2O_4{\cdot}3H_2O$

The thermal analysis results from the evaluation of curves obtained at all heating rates are summarized in Table 1. However, only the curve that is obtained at heating rate of 2 °C/min and in all experiment atmospheres is presented in Fig. 1 as an example. It is found that uranyl oxalate hydrate's decomposition consists of four major steps, first two are endothermic and second two are exothermic. Endothermic reactions are the same in all atmospheres and correspond to dehydration reactions. Two exothermic reactions occur consecutively and determining the temperature range of reactions is very stressful, especially in nitrogen atmosphere.

Reaction temperature ranges are determined by evaluating not only thermograms, but also minimum points of variation of activation energy versus decomposition fraction as shown in kinetic analysis section.

The experimental mass loss percentage (avg. 8.745% in all heating rates and all atmospheres) due to dehydration of two molecules of water (Dh.I reaction) is perfectly compatible with theoretical value (8.742%). $UO_2C_2O_4{\cdot}3H_2O$ starts at 323 K and finishes at 388 K, and dehydration peak temperature is 350.51 K averagely in all atmosphere and heating rates. This reaction is occurred as stated below.

$$UO_2C_2O_4 \cdot 3H_2O_{(s)} \rightarrow UO_2C_2O_4 \cdot H_2O_{(s)} + 2H_2O_{(g)} \quad (Dh.I)$$

Table 1 The mass loss data for the decomposition of $UO_2C_2O_4{\cdot}3H_2O$ in all atmospheres at different heating rates

Reac.	Atmospheric condition	Nitrogen				Air				Oxygen			
	β °C/K	2	4	6	Avg.	2	4	6	Avg.	2	4	6	Avg.
Dh.I	T_i/K	315	320	330	**322**	325	326	328	**326**	311	325	323	**320**
	T_f/K	389	385	403	**392**	361	388	418	**389**	379	387	385	**384**
	T_{peak}/K	337.32	348.56	361.86	**349.25**	349.21	355.60	360.62	**355.14**	339.37	347.40	354.63	**347.13**
	% Δw	8.730	8.743	8.759	**8.744**	8.743	8.750	8.734	**8.742**	8.750	8.747	8.753	**8.750**
Dh.II	T_i/K	389	385	403	**392**	361	388	418	**389**	379	387	385	**384**
	T_f/K	433	442	450	**442**	439	451	459	**450**	429	438	443	**437**
	T_{peak}/K	416.36	425.93	433.40	**425.23**	431.77	441.34	444.44	**439.18**	419.32	427.87	432.5	**426.56**
	% Δw	4.387	4.372	4.358	**4.372**	4.376	4.379	4.363	**4.373**	4.37	4.373	4.359	**4.367**
Dc.I	T_i/K	433	442	450	**442**	439	451	459	**450**	429	438	443	**437**
	T_f/K	605.01	614.17	622.00	**613.73**	609.60	622.20	627.40	**619.73**	615.71	624.00	626.75	**622.15**
	T_{peak}/K	602.91	–	–	**602.91**	606.35	618.43	625.15	**616.64**	609.64	620.33	625.31	**618.43**
	% Δw	6.757	6.798	6.818	**6.791**	6.809	6.646	6.774	**6.743**	6.796	6.784	6.793	**6.791**
Dc.II	T_i/K	605.01	614.17	622.00	**613.73**	609.60	622.20	627.40	**619.73**	615.71	624.00	626.75	**622.15**
	T_f/K	619.00	628.00	635.00	**627.33**	632.00	642.00	646.00	**640.00**	634.20	640.40	643.00	**639.20**
	T_{peak}/K	608.41	618.03	625.96	**617.47**	625.11	635.09	641.33	**633.84**	624.54	633.49	637.32	**631.78**
	% Δw	12.775	12.803	12.787	**12.788**	10.769	10.845	10.670	**10.761**	10.783	10.873	10.652	**10.769**

Bold characters are emphasized average value

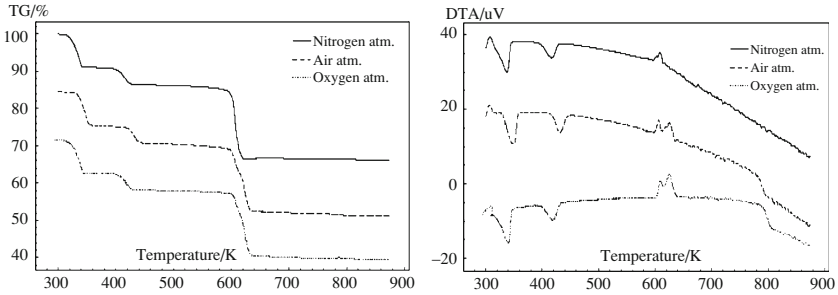

Fig. 1 TG and DTA curves of $UO_2C_2O_4{\cdot}3H_2O$ in all experiment atmosphere at 2 °C/min heating rate

Average dehydration reaction enthalpy is 148.81 or 74.41 kJ/mol water, which is higher than the evaporation enthalpy of the water (40.60 kJ/mol), that the water molecules chemically bounded to the compound.

Second dehydration reaction (Dh.II) starts at 388 K and finishes at 443 K, and reaction peak temperature is 430.33 K averagely in all atmosphere and heating rates. The average experimental mass loss percentage (4.371%) is perfectly compatible with theoretical value (4.371%). This reaction is occurred as stated below.

$$UO_2C_2O_4 \cdot H_2O_{(s)} \rightarrow UO_2C_2O_{4(s)} + H_2O_{(g)} \qquad \text{(Dh.II)}$$

The average reaction enthalpy is 88.81 kJ/mol water, which is higher than first reaction enthalpy. This result confirms that three hydrates are not the same characteristic and one of them bounds the compound more strongly.

Anhydrite uranyl oxalate is stable at the 443–590 K temperature range, and effective decomposition starts after the 600 K. Decomposition stages of anhydrite uranyl oxalate occur in different mechanism in nitrogen atmosphere from air and oxygen atmosphere. In air and oxygen atmosphere, two reactions can be separated with the help of DTA curves although the separation of two reactions is very difficult from TG curves. In nitrogen atmosphere two consecutive reactions can be separated only DTA curve which is taken with 2 °C/min heating rate. If two consecutive physical or chemical events exist, events can be observed as a single event in the thermogram for higher heating rates. To determine temperature ranges of two reactions, we focused on not only decomposition region in TG curves but also we used tendencies of activation energy with respect to the decomposition ratio value in whole decomposition stage that will be explained later sections (Fig. 4b). The TG curves, which are limited with the only decomposition range, in all atmospheres and in 4 °C/min heating rate are presented in Fig. 2.

First decomposition (Dc.I) occurs between temperatures of 443.00 and 618.54 K with peak values between 602.91 and 625.31 K in all atmospheres and heating rates. Dc.I corresponds to the formation of uranyl carbonate intermediate product in all atmospheres and heating rates. The mean value for experimental mass loss percentages (6.775% for all heating rates and all atmospheres) is compatible with theoretical value (6.796%). The proposed reaction equation for this event is given below.

$$UO_2C_2O_{4(s)} \rightarrow UO_2CO_{3(s)} + CO_{(g)}. \qquad \text{(Dc.I)}$$

The Dc.I reaction product CO converts into CO_2 with an exothermic combustion reaction in air and oxygen atmospheres. This reaction is stated as below. While the exothermic peak was observed at 617.54 K in DTA thermograms for air and oxygen atmosphere, it was unable to observe the same peak in nitrogen atmosphere.

$$CO_{(g)} + 1/2O_{2(g)} \rightarrow CO_{2(g)}$$

Unstable uranyl carbonate starts to decompose after a very short period of time (0.5 s) with short temperature increments (1.2 °C) (Figs. 2 and 4b). Decomposition of anhydrite uranyl oxalate has previously been published as a single-stage reaction since the TG thermograms were insufficient to distinguish two separate decomposition stages (5–7).

Decomposition II (Dc.II) occurs exothermically, and UO_3 is appeared to be primary product in all atmospheres and heating rates. This reaction occurs at a temperature range of 621–640 K and approximately at peak temperature value of 632.81 K in air and oxygen atmospheres. The mean value for experimental mass loss percentages (10.765%) is perfectly compatible with theoretical value (10.678%). This reaction is occurred as stated below.

$$UO_2CO_{3(s)} \rightarrow UO_{3(s)} + CO_{2(g)} \qquad \text{(Dc.II)}$$

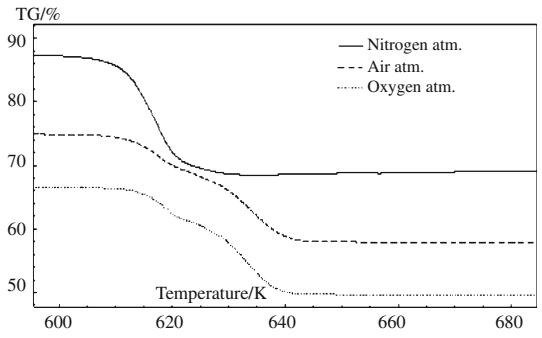

Fig. 2 TG curves, which are focused on decomposition range, with 4 °C/min in all atmosphere

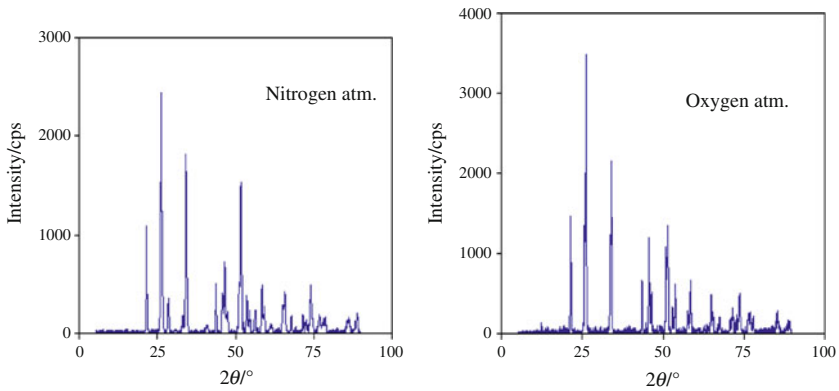

Fig. 3 X-Ray powder diffraction patterns of the final residue of thermal decomposition in nitrogen and oxygen atmosphere

Increasing temperature and the atmospheric conditions convert UO_3 into U_3O_8 which is partially more stable product, in air and oxygen atmosphere (Dc.IIc). Results of X-Ray powder diffraction patterns of the final residue (Fig. 3) and compliance of experimental mass loss percentage value (19.018%) with the theoretical (18.768%) mass loss value confirmed that the final decomposition product is U_3O_8 [17], U_3O_8 File No. 31-1425].

In nitrogen atmosphere, Dc.I reaction product CO partially converts Dc.II solid product UO_3 to UO_2 (Dc.IIa). Due to formation of CO_2 in nitrogen atmosphere (Dc.IIa), Dc.II reaction occurs exothermically and mass loss value (12.788%) within 614–627 K temperature range is larger than that of oxygen atmosphere (10.765). Increasing temperature and the atmospheric conditions initially degrade UO_3 into UO_2 and then convert into U_2O_5 evidently. Final product is partially more stable in flowing nitrogen atmosphere (Dc.IIb). Results of X-Ray powder diffraction patterns of the final product (Fig. 3) and harmony of experimental mass loss percentage value (19.579%) with the theoretical (19.415%) mass loss value proved us that final decomposition product is U_2O_5 [17, U_2O_5 File No. 32-1403].

$$UO_{3(s)} + CO_{(g)} \rightarrow UO_{2(s)} + CO_{2(g)} \quad \text{(Dc.IIa)}$$

$$UO_{3(s)} + UO_{2(s)} \rightarrow U_2O_{5(s)} \quad \text{(Dc.IIb)}$$

$$2UO_{3(s)} + UO_{2(s)} \rightarrow U_3O_{8(s)} \quad \text{(Dc.IIc)}$$

Kinetic analysis of $UO_2C_2O_4{\cdot}3H_2O$

First, we have studied a combination of dehydration I and dehydration II reactions to determine temperature ranges exactly. Figure 4a presents the variation of activation energy with respect to the decomposition ratio-α in all atmospheres.

As seen from the Fig. 4a, two reactions are clearly separated. Dh.I and Dh.II reactions temperature and time range were determined using minimum point in E_a–α graphs.

After that separation, the activation energy value of each stages, Dh.I and Dh.II, is calculated using two model-free methods in all atmospheres.

The activation energy values calculated by using two methods are perfectly compatible with each other and present similar variations especially in air atmosphere for Dh.I reaction. The average activation energy values are 40.461, 52.885, and 69.767 kJ/mol in nitrogen, oxygen, and air atmospheres, respectively.

The average activation energy of Dh.II value is higher than Dh.I value in all atmospheres which are 94.318, 129.871, and 135.726 kJ/mol in nitrogen, oxygen, and air atmospheres, respectively. Average Dh.II enthalpy value is higher than Dh.I enthalpy value too. These results prove that three hydrates are different character. Water in monohydrate crystal structure bounds the compound more strongly than water in three hydrate crystal structure and needs higher energy to remove.

After these calculations, we investigated the reaction models with modeling (composite) methods. We selected proper models which have highest regression analysis, lowest standard deviation, and the activation energy value show good agreement to those obtained from model-free KAS and FWO equations. Calculated activation energy, standard deviation, and regression analysis values from first two models that best fit to Dh.I and Dh.II reactions were presented in Table 2. For comparison, activation energy values, which were calculated model-free KAS and FWO equations, were also presented in the same table.

The most proper model equation is A_3 for Dh.I in all atmospheres. While A_2 model equation is proper in nitrogen and air atmosphere, $A_{1.5}$ model equation is proper in oxygen atmosphere for Dh.II reaction. These model equations correspond to nucleation and growth mechanism. In literature most of dehydration reactions were explained with nucleation and growth mechanism [18–20]. As an example, the most proper model graphs of Dh.II reaction in all experiment atmospheres are presented in Fig. 5.

The other thermodynamic parameters were calculated from best fits model equations and were tabulated in Table 3.

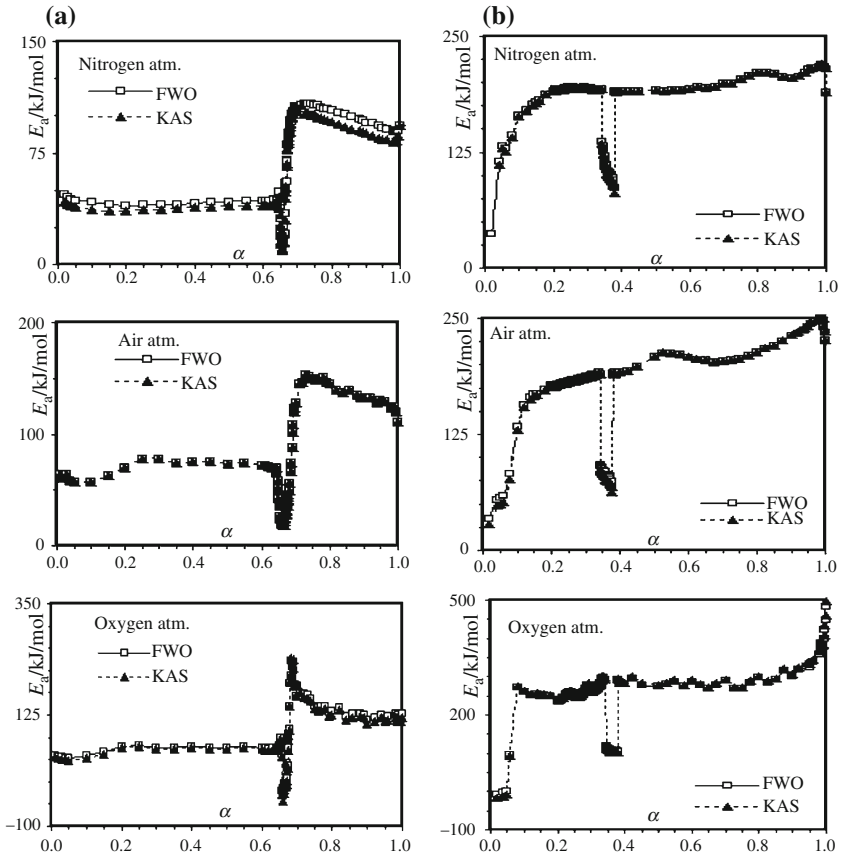

Fig. 4 Variation of activation energy values of dehydration (**a**) and decomposition (**b**) reactions with α in all atmosphere

Table 2 The average activation energy value which calculated with Composite Methods and Model Free Methods (KAS–FWO) for Dh.I and Dh.II reactions

Reac.			Composite method I				Composite method II			
	Atmospheric condition	Model	R^2	S	E_a/kJ/mol	KAS E_a/kJ/mol	R^2	S	E_a/kJ/mol	FWO E_a/kJ/mol
Dh.I	N_2	A_3	0.992	3.732	38.810	38.703	0.994	3.732	42.386	42.219
		A_4	0.992	5.041	53.667		0.994	4.976	56.514	
	Air	A_3	0.992	8.067	51.459	69.767	0.994	7.643	54.459	69.767
		A_4	0.992	6.058	37.139		0.994	5.732	40.844	
	O_2	A_3	0.987	12.250	51.871	51.430	0.990	11.674	54.908	54.340
		A_4	0.974	7.054	37.806		0.980	6.850	41.339	
Dh.II	N_2	A_2	0.999	8.450	89.553	90.972	0.999	7.920	91.827	97.663
		$A_{1.5}$	0.999	11.226	121.747		0.999	10.560	122.436	
	Air	A_2	0.997	12.323	119.190	135.726	0.997	11.637	120.243	135.726
		$A_{1.5}$	0.997	16.403	161.347		0.997	15.516	160.324	
	O_2	$A_{1.5}$	0.995	10.764	129.079	126.667	0.995	10.149	129.414	133.066
		A_2	0.995	8.095	95.050		0.995	7.611	97.061	

The average calculated value of ΔH^*, ΔS^*, and ΔG^* for Dh.I reaction are 37.705 kJ/mol, −141.945 J/mol K, and 86.747 kJ/mol in nitrogen atmosphere, 50.030 kJ/mol, −107.569 J/mol K, and 87.943 kJ/mol in air atmosphere, 50.528 kJ/mol, −107,569 J/mol K, and 87.943 kJ/mol in oxygen atmosphere, respectively. The entropy of activation (ΔS^*) value for Dh.I is negative in all atmosphere. It means that the corresponding activated complexes were with higher degree of arrangement than the initial state. So the removal of two crystal water may be interpreted a slow stage [21, 22].

For Dh.II reaction stage of the value of ΔH^*, ΔS^*, and ΔG^* are 87.167 kJ/mol, −44.931 J/mol K, and 106.303 kJ/mol in nitrogen atmosphere, 116.070 kJ/mol,

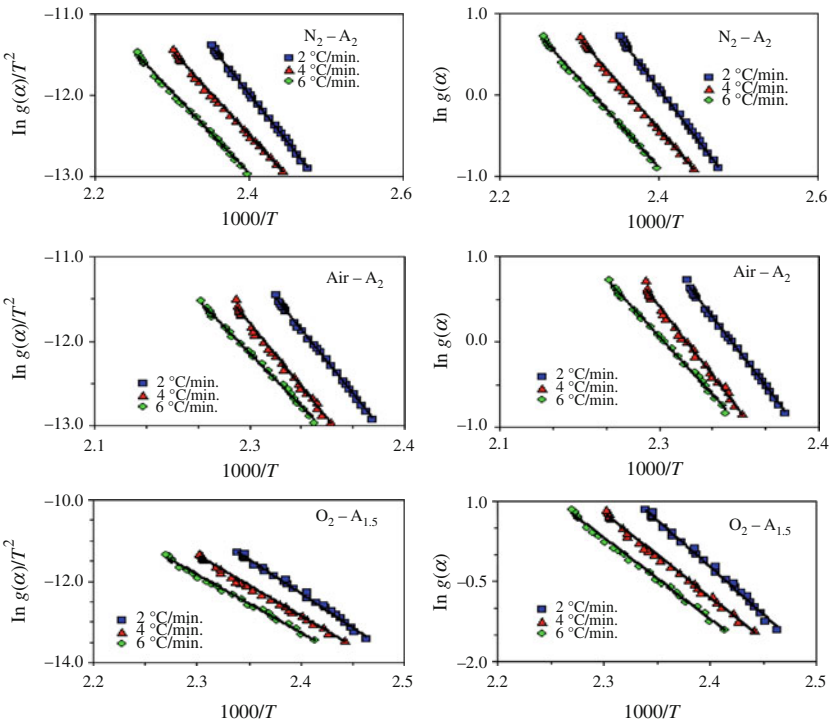

Fig. 5 The most proper model graphs of Dh.II reaction in all atmosphere (*left side* for C.M I and *right side* for C.M II)

Table 3 Thermodynamic parameters of Dh.I and Dh.II reactions

React.	Atmospheric condition	Method	Model	E_a/kJ/mol	ln A	ΔH^*/kJ/mol	ΔS^*/J/mol K	ΔG^*/kJ/mol
Dh.I		C.M I	A_3	38.810	11.685	35.917	−149.040	87.685
	N_2	C.M II	A_3	42.386	13.572	39.493	−133.349	85.809
		C.M I	A_3	51.459	15.9755	48.530	−113.475	88.525
	Air	C.M II	A_3	54.459	17.396	51.530	−101.663	87.361
		C.M I	A_3	51.871	16.494	49.010	−108.972	86.344
	O_2	C.M II	A_3	54.908	17.936	52.046	−96.978	85.264
Dh.II	N_2	C.M I	A_2	89.553	24.028	86.030	−48.058	106.495
		C.M II	A_2	91.827	24.781	88.304	−41.804	106.110
	Air	C.M I	A_2	119.190	31.507	115.543	13.825	109.574
		C.M II	A_2	120.243	31.794	116.596	16.214	109.572
	O_2	C.M I	$A_{1.5}$	129.079	35.452	125.548	46.899	105.733
		C.M II	$A_{1.5}$	129.414	35.523	125.884	47.488	105.812

15.020 J/mol K, and 109.573 kJ/mol in air atmosphere, 125.716 kJ/mol, 47.194 J/mol K, and 105.773 kJ/mol in oxygen atmosphere. While dehydration occurs slowly because of the negative activation entropy in nitrogen atmosphere, the same dehydration occurs fastly due to the positive activation entropy in air and oxygen atmosphere.

Anhydrite uranyl oxalate starts decomposing slowly. Although previous studies suggested that decomposition occured only single step [4–7], our detailed kinetic analysis revealed the decomposition occurred in two steps. Separation of these stages is too difficult. Firstly, we have studied a combination of two decomposition reactions to determine temperature range exactly. We scanned very small α value to ensure the clear separation. Figure 4b presents the variation of activation energy with respect to the decomposition ratio-α in all atmospheres. In all methods and all atmospheres, after $\alpha = 0.342$ value, the activation energy decreases with an increase in decomposition ratio and it reaches to a minimum value for 0.378 decomposition ratio. After reaching to the minimum value, the activation energy increases quickly with the increase in decomposition ratio. We used temperature and time value at $\alpha = 0.378$ decomposition ratio and distinguished of two reaction boundary.

Table 4 The average activation energy value which calculated with Composite Methods and Model-Free Methods (KAS–FWO) for Dc.I and Dc.II reactions

Reac.			Composite method I				Composite method II			
	Atmospheric condition	Model	R^2	S	E_a/kJ/mol	KAS E_a/kJ/mol	R^2	S	E_a/kJ/mol	FWO E_a/kJ/mol
Dc.I	N_2	A_3	0.984	40.075	181.879	188.384	0.986	38.473	181.058	188.767
		A_4	0.973	31.738	133.871		0.961	30.301	136.934	
	Air	A_3	0.998	32.032	164.079	175.941	0.998	30.602	165.716	176.966
		A_4	0.998	23.985	120.505		0.998	22.952	124.287	
	O_2	A_2	0.976	42.488	252.305	253.116	0.978	40.714	249.808	250.395
		A_3	0.971	23.483	161.062		0.975	22.412	162.882	
Dc.II	N_2	A_3	0.989	29.760	211.230	201.173	0.990	28.220	210.972	202.975
		A_4	0.970	25.129	149.256		0.974	23.980	151.676	
	Air	R_2	0.985	22.152	228.213	220.700	0.987	21.224	226.686	219.824
		$A_{1.5}$	0.950	19.883	212.749		0.954	19.008	212.230	
	O_2	R_2	0.992	25.212	290.375	293.311	0.993	24.016	286.041	288.801
		$A_{1.5}$	0.976	23.042	270.659		0.978	21.948	267.296	

After that separation, the activation energy value of each stages, decomposition I (Dc.I) and decomposition II (Dc.II), calculated using different methods in all atmosphere. The average activation energy values are 167.989, 182.053, and 245.742 kJ/mol in air, nitrogen, and oxygen atmospheres, respectively, for Dc.I reaction.

Dc.II reaction corresponds to degradation of uranyl carbonate intermediate product and needs higher energy. Dependence of activation energy values with respect to decomposition ratio (α) is different in all atmosphere. Average activation values are 202.733, 212.813, and 289.569 kJ/mol in nitrogen, air, and oxygen atmospheres, respectively.

After these calculations, regardless of the model, we investigated the reaction models and calculated other thermodynamic parameters. Calculated activation energy, standard deviation, and regression analysis values from first two models that best fit to Dc.I and Dc.II reactions were presented in Table 4. For comparison, activation energy values, which were calculated model free KAS and FWO equations, were also presented in the same table.

While A_3 model equation is proper in nitrogen and air atmosphere, A_2 model equation is proper in oxygen atmosphere for Dc.I reaction. Dc.II reaction occurs with different kinetic model (A_3) in nitrogen atmosphere from air and oxygen atmospheres (R_2).

In nitrogen atmosphere, CO released from Dc.I has facilitated formation of the U_2O_5 which is the final product of the Dc.II reactions. For this reason, activation energy and activation enthalpy value in nitrogen atmosphere is lower than same thermodynamic value in air and oxygen atmosphere.

Table 5 Thermodynamic parameters of Dc.I and Dc.II reactions

React.	Atmospheric condition	Method	Model	E_a/kJ/mol	ln A	ΔH^*/kJ/mol	ΔS^*/J/mol K	ΔG^*/kJ/mol
Dc.I	N_2	C.M I	A_3	181.879	33.731	176.795	29.557	158.355
		C.M II	A_3	181.058	33.572	175.974	28.232	158.387
	Air	C.M I	A_3	164.079	29.978	158.967	−1.692	159.675
		C.M II	A_3	165.716	30.319	160.604	1.145	159.585
	O_2	C.M I	A_2	252.305	47.286	247.175	142.183	159.218
		C.M II	A_2	240.808	46.847	244.679	138.530	158.983
Dc.II	N_2	C.M I	A_3	211.230	39.730	206.086	79.355	156.893
		C.M II	A_3	210.973	39.668	205.841	78.841	156.963
	Air	C.M I	R_2	228.213	41.294	222.948	92.142	164.471
		C.M II	R_2	226.686	40.991	221.421	89.622	164.546
	O_2	C.M I	R_2	290.375	53.438	285.130	193.142	163.216
		C.M II	R_2	286.041	52.721	280.796	187.182	162.644

The other thermodynamic parameters of these reactions, which were calculated using proper model equations, were presented in Table 5.

Activation entropy values of the Dc.II reaction are positive in all atmosphere and heating rates. This indicates a malleable activated complex that leads to a large number of degrees of freedom of rotation and vibration. These results may be interpreted as a ''fast'' stage [21, 22]. The positive value of ΔG^* for the decomposition stage shows that it is connected with the introduction of heat and it is non-spontaneous process.

Conclusions

Thermal decomposition of the $UO_2C_2O_4{\cdot}3H_2O$ was studied thermogravimetrically in nitrogen, air, and oxygen atmosphere. It is found that the compound decomposes in four stages which correspond to dehydration (two) and decomposition (two) reactions. Reaction temperature ranges are determined by evaluating not only thermograms, but also minimum points of variation of activation energy versus decomposition fraction.

While Dh.I and Dh.II reactions are the same mechanism in all atmospheres, atmospheric conditions are very important for Dc.I and Dc.II reactions. Decomposition reactions consist of two stages which is determined first in this article. The first decomposition reaction corresponds to occur as uranyl carbonate intermediate product. This reaction product (UO_2CO_3) and temperature range are not dependent on the atmospheric conditions but reactions of released gas changes with atmosphere. In air and oxygen atmospheres, Dc.I gas product (CO) converts into CO_2 with an exothermic combustion reaction. In nitrogen atmosphere, same reaction was not observed. Atmospheric conditions have been effective in the formation of final decomposition products for Dc.II reaction. This reaction occurs in two sub-stages. Firstly, UO_3 oxide product is obtained from degradation of uranyl carbonate in all atmospheres, and secondly UO_3 converts to more stable products depending on the atmospheric conditions (U_2O_5 in nitrogen atmosphere, U_3O_8 in air and oxygen atmosphere). Final decomposition products are confirmed by X-Ray diffraction patterns.

All of these reaction stages were investigated in a detailed way. The activation energies of the dehydrations and decompositions were calculated using the model-free equations; the KAS and FWO methods. Activation energy values calculated by these two methods are compatible with each other.

The kinetic model equations which described the reactions are determined. Activation energy values which are calculated from proper model equations and methods (C.M I and C.M II) show good agreement with activation energies calculated from model-free equations (KAS and FWO). The other thermodynamic parameters were calculated from proper model equations. These thermodynamic functions are consistent with kinetic parameters.

These data will be important for further studies of the studied compound and are applied to solve various scientific and practical problems involving the participation of solid phases.

Acknowledgements The authors gratefully thank the 107T293 (TBAG-HD/282) and 2009FBE001 projects.

References

1. Duvieubourg L, Nowogrocki G, Abraham F, Grandjean S. Hydrothermal synthesis and crystal structures of new uranyl oxalate hydroxides: α- and β-$[(UO_2)_2(C_2O_4)(OH)_2(H_2O)_2]$ and $[(UO_2)_2(C_2O_4)(OH)_2(H_2O)_2]{\cdot}H_2O$. J Solid State Chem. 2005;178:3437–44.
2. Aybers MT. Kinetic study of the thermal decomposition of thorium oxalate dehydrate. J Nucl Mater. 1998;252:28–33.
3. Dollimore D, Jones LF, Nicklin T, Spooner P. Thermal decomposition of oxalates. Part 13. Surface area Changes in the thermal decomposition of uranyl oxalate. J Chem Soc Faraday Trans. 1973;69(1):1827–33.
4. Tel H, Bülbül M, Eral M, Altaş Y. Preperation and characterization of uranyl oxale powders. J Nucl Mater. 1999;275:146–50.
5. Dahale ND, Chawla KL, Jayadevan NC, Venugopal V. X-ray, thermal and infrared spectroscopic studies on lithium and sodium oxalate hydrate. Thermochim Acta. 1997;293:163–6.
6. Dahale ND, Chawla KL, Venugopal V. X-ray, thermal and infrared spectroscopic studies on potassium, rubidium and caesium uranyl oxalate hydrate. J Therm Anal Calorim. 2000;61:107–17.
7. Rodante F, Vecchio S, Materazzi S, Vasca E. Kinetic and thermodynamic study of the $Na_4(UO_2)_2(OH)_4(C_2O_4)_2$ complex. Int J Chem Kinet. 2003;35:661.
8. Ozawa T. Kinetic analysis of derivative curves in thermal analysis. J. Thermal Anal. 1970;2:301.
9. Küçük F, Yildiz K. The decomposition kinetics of mechanically activated alunite ore in air atmosphere by thermogravimetry. Thermochim Acta. 2006;448:107–10.
10. Cilgi GK, Cetişli H. Thermal decomposition kinetics of aluminum sulfate hydrate. J Therm Anal Calorim. 2009;98:855–61.
11. Boonchom B. Kinetic and thermodynamic studies of $MgHPO_4{\cdot}3H_2O$ by non-isothermal decomposition data. J Therm Anal Calorim. 2009;98:863–71.
12. Ocakoğlu K, Emen FM. Thermal analysis of *cis*-(dithiocyanato) (1,10-phenanthroline-5,6-dione) (4,4′-dicarboxy-2,2′-bipyridyl) ruthenium(II) photosensitizer. J Therm Anal Calorim. 2011;104:1017–22.
13. Gabal MA. Non-Isothermal studies for the decomposition course of CdC_2O_4–ZnC_2O_4 mixture in air. Thermochim Acta. 2004;412:55–62.
14. Budrugeac P, Segal E. On the use of Diefallah's composite integral method for the non-isothermal kinetic analysis of heterogeneous solid-gas reactions. J Therm Anal Calorim. 2005;82:677–80.
15. Wendlant Wesley WM. Thermal analysis. 3rd ed. New York: Wiley; 1986.
16. Vyazovkina S, Burnhamb AK, Criadoc JM, Pérez-Maquedac LA, Popescud C, Sbirrazzuolie N. ICTAC kinetics committee

recommendations for performing kinetic computations on thermal analysis data. Thermochim Acta. 2011;520:1–19.
17. The International Centre for Diffraction Data File No. 31-1425 and 32-1403.
18. Favergeon L, Pijolat M, Helbert C. A mechanism of nucleation during thermal decomposition of solids. J Mater Sci. 2008;43: 4675–83.
19. Galwey AK, Spinicci R, Guarini GT. Nucleation and growth process occurring during the dehydration of certain alums: the generation, the development and the function of the reaction interface. Proc R Soc Lond A. 1981;378:477.
20. Koga N, Tanaka H. A physico-geometric approach to the kinetics of solid-state reactions as exemplified by thermal dehydration and decomposition of inorganic solids. Thermochim Acta. 2002;388: 41–61.
21. Boonchom B, Danvirutai C. Kinetics and thermodynamics of thermal decomposition of synthetic $AlPO_4 \cdot 2H_2O$. J Therm Anal Calorim. 2009;98:771–7.
22. Boonchom B. Kinetics and thermodynamic properties of the thermal decomposition of manganese dihydrogenphosphate dihydrate. J Chem Eng Data. 2008;53:1553–8.